IEEE Access
Multidisciplinary | Rapid Review | Open Access Journal

Received January 20, 2022, accepted February 5, 2022, date of publication February 7, 2022, date of current version February 16, 2022.

Digital Object Identifier 10.1109/ACCESS.2022.3149925

Neckband-Based Continuous Blood Pressure Monitoring Device With Offset-Tolerant ROIC

KWANGMUK LEE[1], (Student Member, IEEE), YUMIN KANG[2], CHAN SAM PARK[1], (Student Member, IEEE), HYUNJOONG KIM[1], (Student Member, IEEE), DAE SIK KEUM[3], DONG PYO JANG[2], AND JAE JOON KIM[1], (Senior Member, IEEE)

[1]Department of Electrical Engineering, Ulsan National Institute of Science and Technology (UNIST), Ulsan 44919, South Korea
[2]Department of Biomedical Engineering, Hanyang University, Seoul 04763, Republic of Korea
[3]SOSO H&C, Daegu 41566, Republic of Korea

Corresponding authors: Dong Pyo Jang (dongpjang@hanyang.ac.kr) and Jae Joon Kim (jaejoon@unist.ac.kr)

This work was supported in part by the National Research Foundation of Korea (NRF) under Grant 2021M3E5D2A01022391; in part by the Institute of Information and Communications Technology Planning and Evaluation (IITP) by the Ministry of Science and ICT (MSIT), South Korea, under Grant 2021-0-00866-001; in part by the Technology Innovation Program through the Alchemist Project by the Ministry of Trade, Industry and Energy (MOTIE), South Korea, under Grant 20012461; and in part by Samsung Electronics.

This work involved human subjects or animals in its research. Approval of all ethical and experimental procedures and protocols was granted by Ulsan National Institute of Science and Technology (UNIST) Institute Review Board under Application No. UNISTIRB-17-12-G.

ABSTRACT This study presents a wearable neckband device for continuous cuffless blood pressure (BP) monitoring, where reliable neck-based BP measurement is achieved by utilizing the electrocardiogram (ECG) and impedance plethysmogram (IPG). Optimal composition and position of sensing electrodes around the neck were decided with consideration for physiological characteristics of the human body, and the core parameter of IPG magnitude was experimentally selected to improve the BP estimation accuracy. For its small-featured noises-tolerant detection capability, a customized readout integrated circuit (ROIC) was developed, which includes two kinds of analog front-ends (AFEs) for biopotential and bio-impedance. Both AFEs are proposed to include an attenuator-assisted hybrid DC-servo loop (DSL) structure, achieving precise pulse transit time (PTT) calculation by lowering the high-pass filtering cutoff frequency and also stable signal acquisition by widening the offset-cancellation range. Real-time PTT monitoring and BP estimation are wirelessly conducted, and its continuous operation time with 350-mAh battery capacity is longer than 5 hours. Efficacy of the proposed neckband BP device was evaluated for 8 healthy subjects under the physical stress condition, where the mean correlation coefficient and the standard deviation were achieved as 0.8508 and 4.17mmHg respectively.

INDEX TERMS Neckband device, pulse transit time, continuous blood pressure monitoring, impedance plethysmogram, readout integrated circuit.

I. INTRODUCTION

Blood pressure (BP) is a primary vital sign in clinical assessments to clarify cardiovascular conditions, and it is a kind of dynamic physiological index which is closely affected by physical and mental states or activities. Thereby, the continuous BP monitoring (CBPM) has significant clinical value for cardiovascular disease diagnosis or prevention. While the catheter-based invasive method is the gold standard, daily-life healthcare monitoring applications prefer non-invasive methods, especially, cuffless CBPM methods [1].

Recently, the pulse morphology of photoplethysmogram (PPG) has been used to estimate the BP. It extracts correlation parameters such as amplitude [2] and steepness [3] from the PPG, and then it provides the BP estimation based on its empirical correlation relationship that is obtained from a lot of experiments in advance. This method is convenient to measure it by utilizing only single PPG device, but there is a difficulty in continuous feature extraction because it is critically vulnerable to noises and motion artifacts. As another CBPM, the tonometry method measures the BP by applying

The associate editor coordinating the review of this manuscript and approving it for publication was G. R. Sinha.

pressures to the artery located near the skin such as radial artery. Although it has been adopted to portable devices such as wrist band, but it is sensitive to misaligned sensing position and body movement, also giving long-lasting uncomfortable pressures on the artery [4].

For better comfort of wearing, the pulse transit time (PTT) based BP estimation is an attractive method, which provides stable measurement and high correlation with the BP [5], [6]. PTT is the time delay between two synchronized pulse waves from proximal and distal sites along the arterial tree, and it is extracted to estimate the BP through pre-calibrated equations or learning-based methods. For its timing extraction, a peak point of the bio-signal has been chosen as a prominent feature compared to others such as pulse morphology since it can easily extract the peak even in unstable sensing conditions. This PTT-based BP estimation has been mostly performed by utilizing electrocardiogram (ECG) and PPG because of their comfortable detectability, even though it effectively corresponds to the pulse arrival that includes the pre-ejection period (PEP) [7]. Additionally, many studies pursued watch-type devices for convenient wearing [8], [9], but they were not suitable for long-time CBPM because subjects are forced to maintain certain postures for measurement.

While the PPG has been widely adopted to measure the pulse wave at the distal site, recent works have utilized the impedance plethysmogram (IPG) to improve the sensitivity of sensing position and also to reduce the power consumption. An IPG-based neck patch device [10] was proposed for BP measurement. However, due to its pulse morphology-based limitation, it is necessary to maintain a sitting posture. Its measurement device was implemented with discrete components or chips, resulting in large size and high power consumption. Another PTT-based BP estimation method [11] utilized the wrist IPG and the finger PPG. Even though it is focused on detection feasibility without compact wearable device implementation, it improved the accuracy by applying a parameter of IPG magnitude.

To achieve various requirements of the CBPM wearable device such as miniatured device integration, low-power consumption and stable signal acquisition, its optimized readout integrated circuit (ROIC) is preferred [12], [13]. Desired bio-signal levels are relatively very small, especially compared to DC-artifacts such as input DC offset (IDO) in biopotential sensing and baseline impedance in bio-impedance sensing. Therefore, appropriate DC-artifact cancellation schemes are necessary in the ROIC design. The DC-servo loop (DSL) method is widely used for DC-artifact cancellation by implementing effective high-pass filtering (HPF) characteristic [14]. However, for wide DC-cancellation range, the HPF cutoff frequency should increase, which causes unwanted signal distortion and inaccurate PTT calculation.

This work presents a compact and user-friendly CBPM device where a neckband-based PTT-BP measurement method is proposed for stable signal acquisition during daily-life wearing. Optimal electrode positions around the neck are located according to physiological characteristics of the human body, and its BP estimation algorithm is also developed to use PTT and IPG magnitude. Its customized ROIC is developed to integrate biopotential and bio-impedance analog front ends (AFEs). It provides wide DC-artifact cancellation capability by applying a proposed attenuator-assisted hybrid-DSL structure which makes the HPF cutoff frequency low enough to obtain precise PTT and the DC-cancellation range wide enough to guarantee stable signal acquisition. A proposed wearable neckband device prototype was manufactured together with a BP estimation algorithm, and its CBPM feasibility was experimentally measured on 8 subjects under the physical stress condition.

II. METHOD

A. ELECTRODES POSITION ON A NECK FOR BIO-SIGNAL SENSING

A signal pair of ECG and PPG has been widely used to measure the PTT by detecting the ECG R-peak and PPG peak [5], [15], but this study is aimed to measure the PTT using ECG and IPG signals for stable signal acquisition around a neck. Since amplitude and shape of bio-signals differ considerably depending on locations of their sensing electrodes, it is necessary to select the optimal sensing positions on the neck. Fig.1(a) shows electrode and sensing positions for measurement of bio-signals on the neck. ECG is generated by the depolarization of polarized heart cells, and it starts at the SA node and passes through the atria, atrioventricular node, and Perkinje fibers to the ventricle. Since the heart is tilted forward to the left in the center of the thoracic cavity, when measuring ECG on the neck, it is possible to obtain a large potential difference by placing the ECG sensing electrodes relatively near and far from the heart.

The blood volume in the blood vessels changes periodically due to the heartbeat, and IPG is obtained by differentiating the measured bio-impedance from the changed blood volume. Two pairs of electrodes are needed to measure the bio-impedance, where one pair of is used to inject AC current on the body and the other is used to sense voltage difference caused by the AC current. Since the carotid artery is symmetrically located at a position inclined forward from the center of the neck, it is possible to obtain large IPG signal by placing each electrode for current injection and voltage measurement on each side of the neck. PPG is measured by using a pair of LED and photodiode, where it is obtained by monitoring the intensity of the reflected light from the LED depending on the blood flow of the blood vessel. It is usually measured at locations where the skin tissue is thin and capillaries are distributed on the skin surface such as finger or earlobe. In this study, the PPG was measured around the neck skin tissue considering the design of the wearable device.

Fig.1(b) shows measured bio-signals on the neck using the BIOPAC (MP160, ECG100C, NICO100C, PPG100C) equipment at the above-mentioned electrode and sensing positions, and chest ECG was additionally measured by attaching

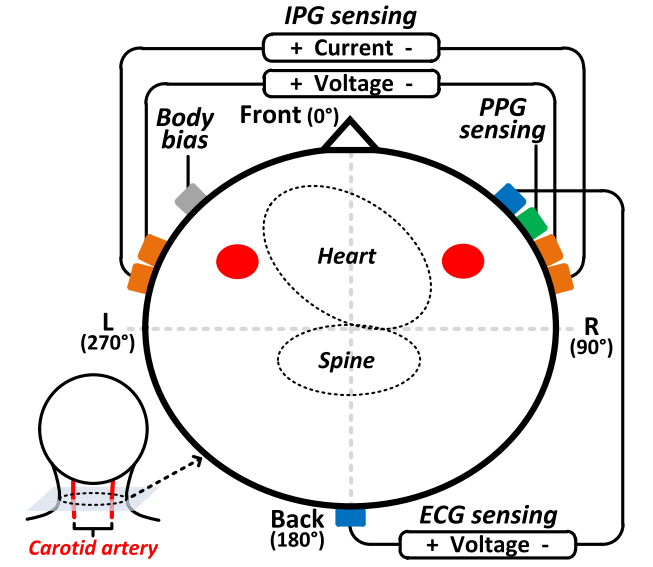

(a)

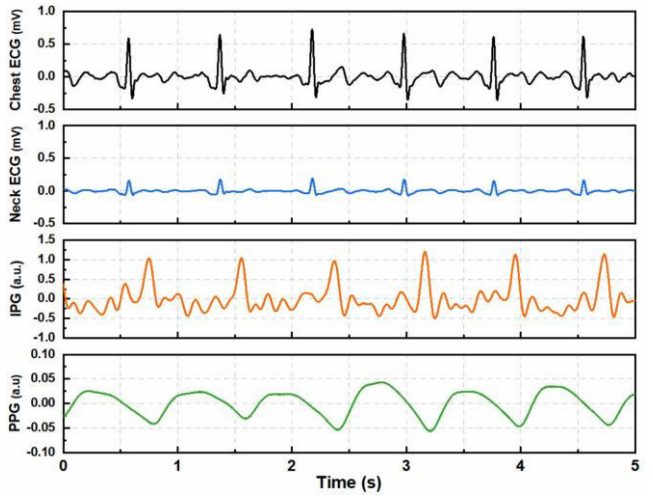

(b)

FIGURE 1. (a) Electrode positions for ECG, IPG, and PPG measurement on a neck and (b) simultaneously measured waveforms of chest ECG, neck ECG, neck IPG, and neck PPG.

electrodes to the Lead I position. Although the neck-ECG has much smaller amplitude than the chest ECG, the R-peak position to indicate the time of ventricular contraction is almost the same.

B. PTT-BASED BP ESTIMATION ALGORITHM

The PPG is a kind of non-invasive method that detects the amount of change in the volume of blood vessels according to the heartbeat on the skin surface. Blood vessels distributed on the skin surface are classified as peripheral blood vessels, which are located on far from the heart such as capillaries [16]. Central aortic pressure reflects the actual load on the heart and aorta [17], and the BP waveform of the carotid artery is similar to that of the aorta because of less pressure distortion [18]. Therefore, it is important to monitor changes in the central arterial vessels close to the heart. The IPG is non-invasively measured by detecting the change of body impedance. Therefore, if the IPG is measured around the neck, it is possible to obtain more accurate PTT than the conventional one calculated from ECG and PPG because the IPG signal is induced from blood volume changes in the carotid artery [19].

As shown in Fig.2(a), five feature points were extracted from IPG and PPG waveforms, and BP estimations were conducted by using ten kinds of PTTs, and the BP estimation accuracy from ECG-PPG and ECG-IPG pairs was compared. The five feature points are the minimum (min), the maximum (max), the maximum of the first derivative (1st_dev_max), and the maximum and the minimum of second derivative value (2nd_dev_max, 2nd_dev_min). Magnitudes of IPG and PPG (MAG_{IPG}, MAG_{PPG}) are the difference of the maximum and minimum values of each waveform.

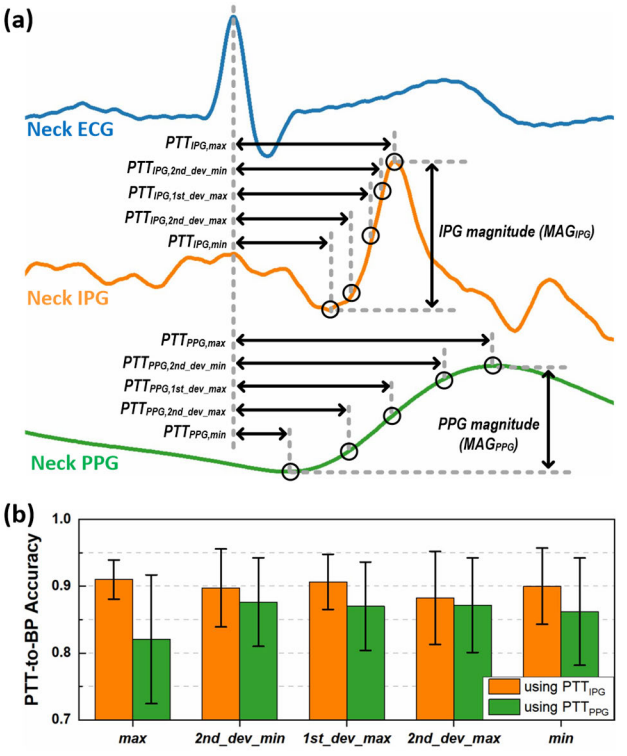

FIGURE 2. (a) Various pulse transit time values which are obtained from the time difference between the ECG R-peak and five feature points of the IPG and PPG waveforms. (b) Accuracy of the BP estimation algorithm between the PTTIPG and PTTPPG with five feature points.

Fig.2(b) shows the correlation coefficient between the reference BP and the estimated BP with IPG and PPG signals depending on the five feature points, where the experiment was conducted for 9 subjects of healthy men with 24-33 ages. The reference BP was measured using the Hartmann automatic sphygmo-manometer (Hartmann Temsoval Duo Control) and the BP estimation was performed using the

following equation:

$$\mathrm{BP_{est}} = \mathrm{a} + \frac{b}{PTT^2} + \mathrm{c} \cdot \exp(MAG_{IPG/PPG}) \qquad (1)$$

The estimated BP from the IPG-based PTT ($\mathrm{PTT_{IPG}}$) has higher correlation coefficient than the BP from the PPG-based PTT ($\mathrm{PTT_{PPG}}$) on the whole feature points. Among the results with the $\mathrm{PTT_{IPG}}$, the BP estimation accuracy is highest when the PTT is obtained from the ECG R-peak and the maximum of the IPG ($\mathrm{PTT_{IPG,max}}$) (Mean±SEM; 0.909±0.009).

III. HARDWARE IMPLEMENTATION

A. OVERVIEW OF NECK-BAND DEVICE AND SENSOR SYSTEM

Fig.3(a) shows an integrated neckband device which includes a sensor module, a 3-D printed neckband frame, a battery, and electrodes. Seven electrodes are positioned to measure the ECG and IPG signals, and the sensor module and battery are positioned in cavities of the neckband frame located on both sides of the ECG+ electrode. This device is convenient for continuous bio-signal acquisition because they don't require additional actions such as touching electrodes by hand, therefore, it helps to monitoring the continuous blood pressure.

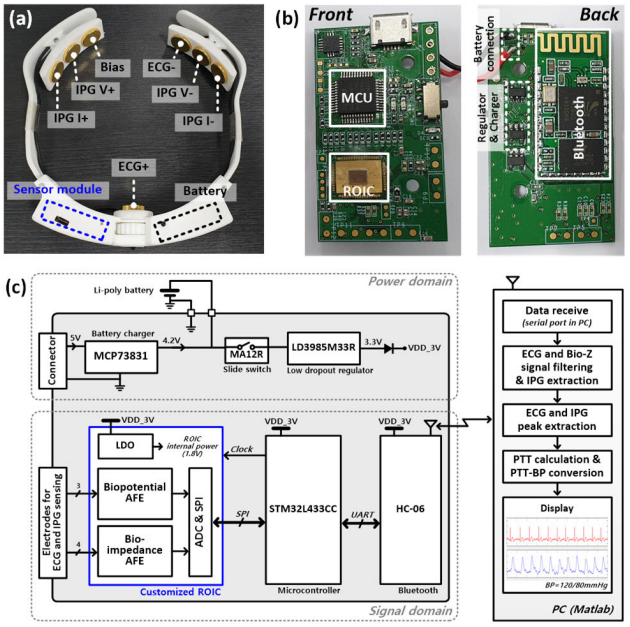

FIGURE 3. (a) Photograph of a developed neckband device and (b) a sensor module. (c) Block diagram of the sensor system for continuous BP monitoring.

Fig.3(b) shows a photograph of the sensor module designed in the size of 2.3cm × 4cm. Fig.3(c) shows a block diagram of the sensor system for continuous BP monitoring, where the sensor module is divided into a power domain and a signal domain. The power domain consists of a micro-USB connector, a battery charger (MCP73831), a lithium-polymer battery, a slide switch (MA12R), and a low-drop-out regulator (LD3985M33R), where the supply voltage of the LDO output drives the signal domain. Signal domain consists of a customized readout integrated circuit (ROIC), a micro-controller (MCU), and bluetooth module (HC-06). The ROIC and MCU exchange data by serial peripheral interface (SPI), and the MCU transmits data according to UART protocol to bluetooth module, which is wirelessly transmitted to PC. Matlab tool processes and visualizes the received data in the PC. ECG and bio-impedance signals sampled with 250 sample/s are filtered, and IPG is extracted by differentiating the bio-impedance signal. Peak extraction of the ECG and IPG, PTT calculation, and PTT-to-BP conversion are sequentially performed. The ECG and IPG waveforms and the calculated BP are displayed in real-time.

B. ARCHITECTURE OF CUSTOMIZED ROIC

Fig.4(a) shows an architecture of the customized ROIC, and it mainly includes biopotential [20] and bio-impedance analog front-ends, and a successive approximation register analog-to-digital converter (SAR-ADC) [21]. The biopotential and bio-impedance AFEs acquire the ECG and bio-impedance signals at each, and SAR-ADC simultaneously converts the bio-signals to digital data. The SPI block controls the ROIC operation using received data from the MCU and transfers the obtained data to the MCU. Fig.4(b) shows a micrograph of the ROIC which was fabricated using a 0.18-μm complementary metal-oxide semiconductor (CMOS) process, and its chip size is 2.8 mm × 2.3 mm.

When measuring the biopotential signal, input DC offset (IDO) voltage is significantly larger than the desired ECG signal [22]. The IPG signal is a very small AC impedance ($< 1\Omega$), but a very large DC impedance ($>$ hundreds Ω) due to the body component is also measured when the IPG signal acquisition [23]. Therefore, DC-artifact cancellation scheme is necessary to sufficiently amplify the desired biopotential and bio-impedance signals, and an analog DC-servo loop (DSL) [14], [20] is a widely used circuit structure to remove the DC artifacts by implementing a HPF characteristic. However, there is a trade-off between implementations of the low HPF cutoff frequency and the wide IDO cancellation range, and if the HPF cutoff frequency is not low enough, inaccurate PTT is obtained by a phase shift which degrades an accuracy of the PTT-based BP estimation. Therefore, in this research, an attenuator-assisted hybrid-DSL scheme is proposed to improve the trade-off and it is adapted to biopotential and bio-impedance AFEs as shown in Fig.4(a).

C. IMPLEMENTATION OF BIOPOTENTIAL AND BIO-IMPEDANCE AFES WITH ATTENUATOR-ASSISTED HYBRID-DSL

Fig.5 shows a low-noise amplifier (LNA) which is designed with proposed attenuator-assisted hybrid-DSL scheme and satisfy characteristics of low-noise and DC-cancellation. Conventional analog-DSL is implemented using R-C integrator and has 1st-order HPF characteristic. It can measure the bio-signals without changing the peak position due to signal

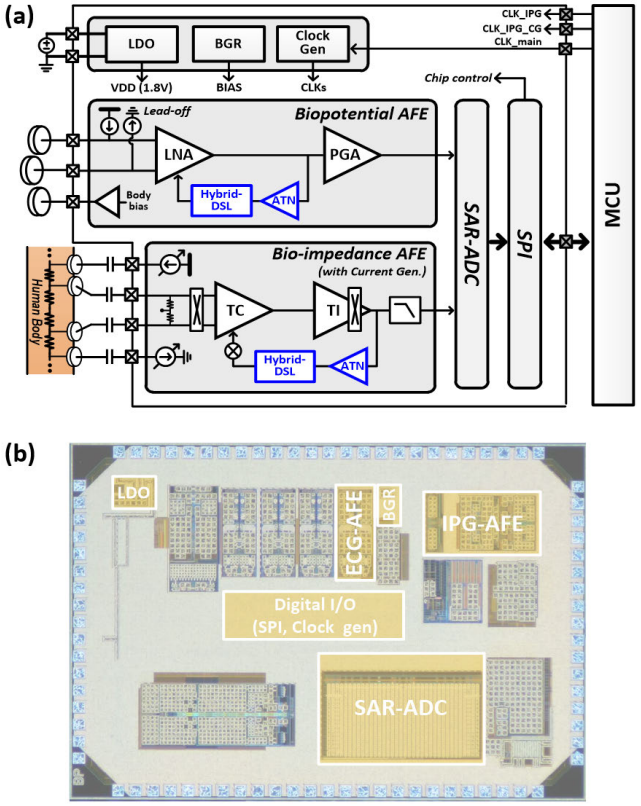

FIGURE 4. (a) Block diagram and (b) micrograph of the customized ROIC.

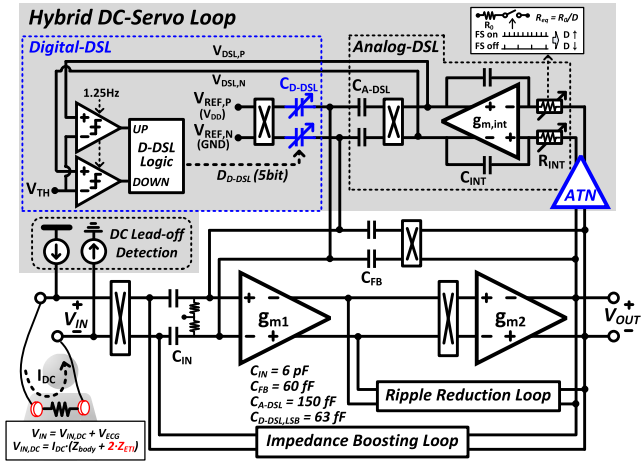

FIGURE 5. Schematic of a low-noise amplifier in the biopotential analog front-end.

distortion and phase shift only when is has a sufficiently lower HPF cutoff frequency (w_{hp}) than the frequency band of the bio-signals. For example, when the w_{hp} and LNA input signal frequency are the same, a 45 degree phase shift occurs which causes a critical error in PTT measurement. Since the ECG and IPG signals generally have a range of 0.5 to tens of Hz, the w_{hp} should be designed much lower than the signal band.

On the other hand, since increasing the integrator capacitor (C_{INT}) increases the chip size too much, techniques such as pseudo-resistor [24] and duty-cycled resistor [25] have been studied to implement a high equivalent resistance in the integrator (R_{INT}) on a small chip area. However, the pseudo-resistor has a large process variation which causes an incorrect w_{hp} implementation. The duty-cycled resistor has a less process variation, but there is a limitation in increasing the equivalent resistance due to the parasitic capacitance of the switch. Therefore, we proposed an attenuator-assisted analog-DSL is proposed, which is a structure in which the attenuator is located on the front of the analog-DSL path. A transfer function of the LNA with the attenuator-assisted analog-DSL is represented in the equation (2).

$$\frac{V_{OUT}}{V_{IN}} = -\frac{C_{IN}}{C_{FB}} \cdot \frac{1}{1 + \frac{\alpha \cdot C_{A\text{-}DSL}}{sR_{INT}C_{INT}C_{FB}}} \tag{2}$$

The HPF cutoff frequency is lowered by multiplying an attenuation coefficient (α), and it is possible to much lower the w_{hp} than the high-resistance implementation techniques because this structure also applies the techniques in the conventional analog-DSL.

Fig.6(a) shows a schematic of the switched-capacitor type attenuator with a fully-differential structure, and Fig.6(b) shows its timing diagram and operation waveforms. In phase 1, C_1 capacitors sample the differential LNA output voltage, and the attenuator output voltages (V_{OUTP}, V_{OUTN}) maintain the sampled voltage in the previous switching period. In phase 2, charge distribution between the C_2 and C_3 capacitors occurs by closing the Φ_1 switches. In phase 3, charge distribution between the C_1 and $C_2 + C_3$ capacitors occurs. At that time, a low-pass filter is implemented by R_1 and $C_1 + C_2 + C_3$ capacitors, and since the closing time of the Φ_2 switch is very short, it can be neglected that the attenuator input voltage is transmitted to the output by driving current from g_{m2} amplifier. Also, the large R_1 resistors limit the output current of g_{m2} amplifier stage to reduce the current requirement. In phase 4, charge distribution between the C_2 and C_3 capacitors occurs by closing the cross-coupled Φ_3 switches are closed. Because the timing diagram is synchronized with a clock frequency of the duty-cycled resistor (f_{DSL}), the attenuator operation can be regarded as a discrete time periodic signal and the attenuation coefficient (α) is calculated as follow equation (3):

$$\alpha = \frac{V_{OUTP,N}}{V_{INP,N}} = \frac{C_1(C_2 - C_3)}{C_1C_2 + C_1C_3 + 4C_2C_3} \tag{3}$$

The C_1~C_3 capacitors are determined to 105fF, 820fF, and 410fF in the implementation of the attenuator, which represents the calculated attenuation coefficient is 0.0292.

Conventional analog-DSL was used to compensate for the potential difference between two input electrodes attached to the body, and generally has a DC-cancellation range of several mV to several tens of mV [25]. On the other hand, DC and AC lead-off detection schemes are frequently used to check whether a signal is continuously measured well [26]. In the AC lead-off detection, since an amplitude caused by

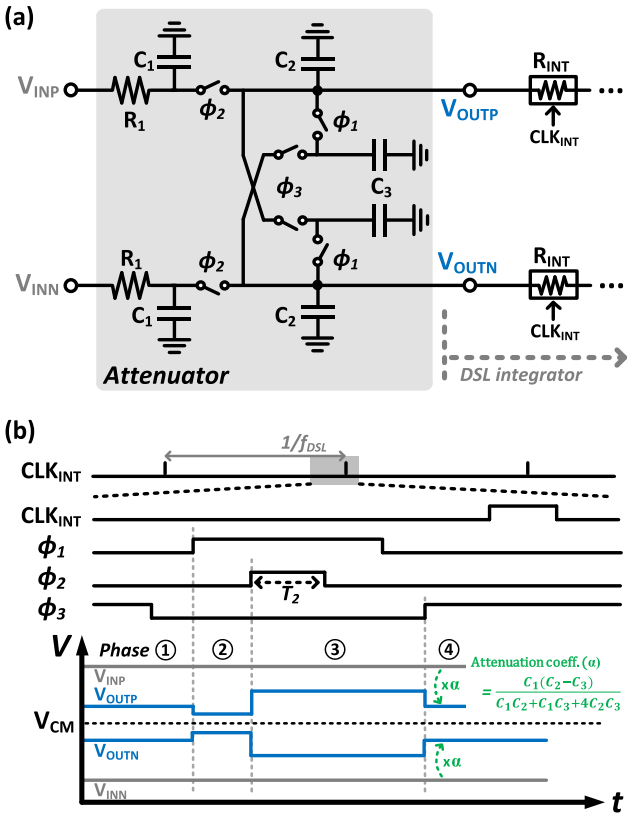

FIGURE 6. **(a) Schematic of the switched-capacitor type attenuator and (b) its timing diagram and operation.**

an input AC current appears at the output of the analog front-end, it must be removed by back-end digital processing. This study applies a DC lead-off detection scheme to minimize system complexity. As shown in the Fig.5, DC current (I_{DC}) flowing across the LNA input generates a potential difference ($V_{IN,DC}$) as it passes through the two electrode-tissue impedances (Z_{ETI}) and body impedance (Z_{body}), and the LNA amplifies the potential difference and bio-signal together. Experimentally, the bio-impedance between both sides of the neck is about 100kΩ at 0Hz current injection. However, Z_{ETI} can be increased to more than hundreds of kilohms due to deterioration of electrode contact condition [27], which requires an additional structure because the analog-DSL cannot compensate the Z_{ETI} induced large offset voltage.

The proposed hybrid-DSL which is a combined structure of the analog-DSL and an additional digital-DSL enables to increase the DC-cancellation range by cancelling the most of IDO voltage in the digital DSL. In this case, the HPF cutoff frequency is maintained because the digital DSL path doesn't affect to the attenuator-assisted analog-DSL operation. Therefore, the ECG signal can be measured by compensating the large IDO voltage even during the lead-off detection operation, and the lead-off condition is determined by monitoring the digital-DSL output (D_{D-DSL}).

In the Fig.5, the digital-DSL consists of two comparators, UP/DOWN counter, and differential capacitor bank (C_{D-DSL}). The LNA output (V_{OUT}) is increased and saturated when the $V_{IN,DC}$ rapidly increases, and an integrator output ($V_{DSL,P}$) gradually increases. When the $V_{INT,P}$ becomes higher than a threshold voltage (V_{TH}), the comparator output (UP) increases the D_{D-DSL} which adjust a connection of C_{D-DSL} to increase the DC-cancellation voltage, and the $V_{IN,DC}$ is compensated through the feedback operation of the hybrid-DSL until the V_{OUT} settles to common-mode voltage. The maximum DC-cancellation range of the hybrid-DSL is determined by a sum of C_{A-DSL} and C_{D-DSL}, and it has an enough range to compensate the IDO because the C_{D-DSL} which consists of the 5bit array of the 63fF unit capacitor is much larger than the C_{A-DSL}.

The integrator output voltage should be completely settled before the D_{D-DSL} is controlled for a stable hybrid-DSL operation, but it has a very long time due to the low HPF cutoff frequency of the attenuator-assisted DSL. Therefore, a fast-settling mode which increase the w_{hp} by reducing the equivalent resistance of the duty-cycled resistor R_{INT} is added to reduce the settling time of analog-DSL when digital-DSL operation is required due to large IDO changes. Fig.7 shows a flow chart and measured transient output of the attenuator-assisted hybrid-DSL with fast-settling mode (MODE_FS). When a large IDO change occurs from +40mV to −60mV, the MODE_FS is activated by sensing the V_{OUT} saturation and the w_{hp} increases. D_{D-DSL} is adjusted until the most IDO is cancelled by the digital-DSL and remained small IDO is also cancelled by the analog-DSL, so the V_{OUT} is recovered to common-mode voltage. The MODE_FS is deactivated 5 seconds after the activation, and the input signal is normally amplified by decreasing the w_{hp}.

Because IPG signal is in the low frequency band and the amplitude of the pulsed AC impedance (R_{AC}) is much smaller compared to the DC baseline impedance (R_{DC}) by the body tissues, there are similar design issues between a bio-impedance AFE and the biopotential AFE. Therefore, the attenuator-assisted hybrid-DSL structure is also applied to the bio-impedance AFE. Fig.8(a) shows a schematic of the bio-impedance AFE which consists of a pseudo-sine current generator, trans-conductance (TC) and trans-impedance (TI) amplifiers, and a feedback loop of a hybrid-DSL. The current generator generates a current with an amplitude of 5-100uApp and a frequency of 62.5kHz (f_{CG}), and only AC current (i_{CG}) flows into the body by the AC-coupling capacitor. (1) Input voltage (V_{IN}) is represented by product of the i_{CG} and body impedances ($R_{DC} + R_{AC}$), and (2) it is demodulated as a chopping frequency (f_{chop}) by the input chopper and transmitted to the TC amplifier. (3) Outputs of the TC and TI amplifiers ($V_{OUT,TC}$, $V_{OUT,TI}$) is proportional to $R_{DC} + R_{AC}$ without the hybrid-DSL, but output saturation occurs at high TC-TI stage gain. (4) Hybrid-DSL is implemented on a TC-stage to prevent the output saturation by cancelling the DC-impedance (R_{DC}), so only the desired AC impedance (R_{AC}) remains. (5) The $V_{OUT,TI}$ is demodulated as a baseband by the output chopper, then only the R_{AC} term which is the target IPG signal remains by filtering the output ripple.

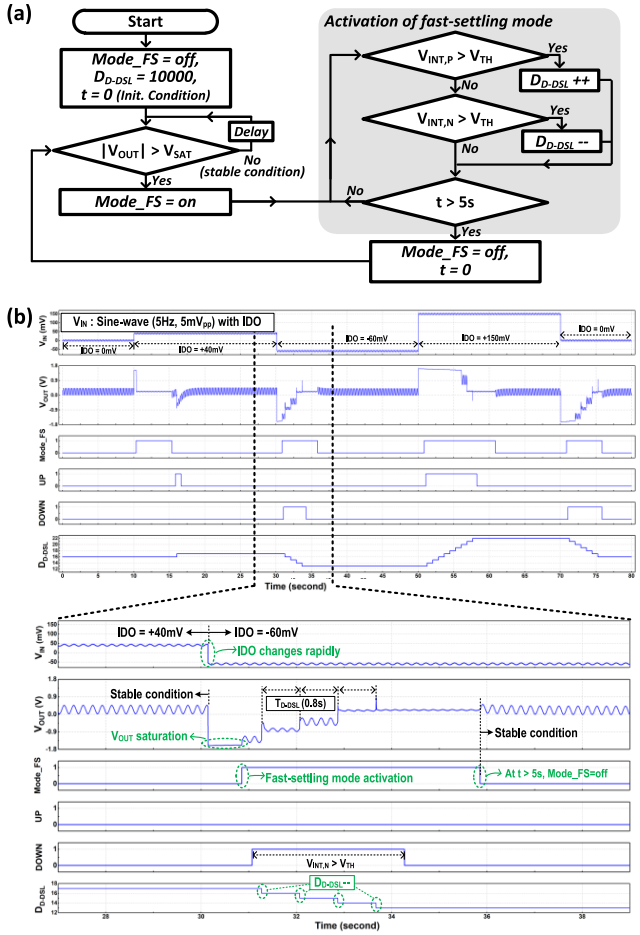

FIGURE 7. (a) Operation flow chart and (b) measured waveform of the fast-settling mode in the digital DSL operation.

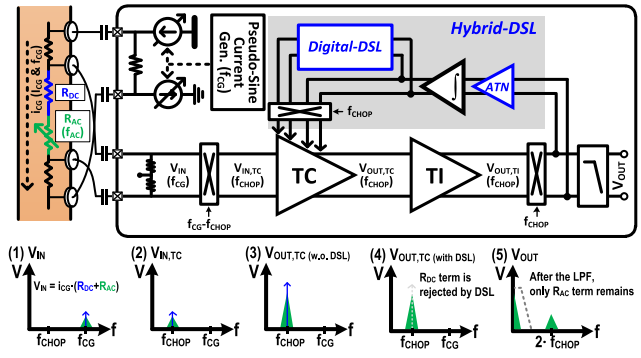

FIGURE 8. Implementation of the bio-impedance analog front-end.

IV. EXPERIMENTAL RESULTS

A. MEASURED RESULTS OF THE CUSTOMIZED ROIC

Fig.9(a) is a measured frequency response of the LNA when the attenuator is deactivated or activated, and it was confirmed that the HPF cutoff frequency was sufficiently lowered by the attenuator. The HPF cutoff frequency is about 1.4Hz on a deactivated condition, but it is lowered than

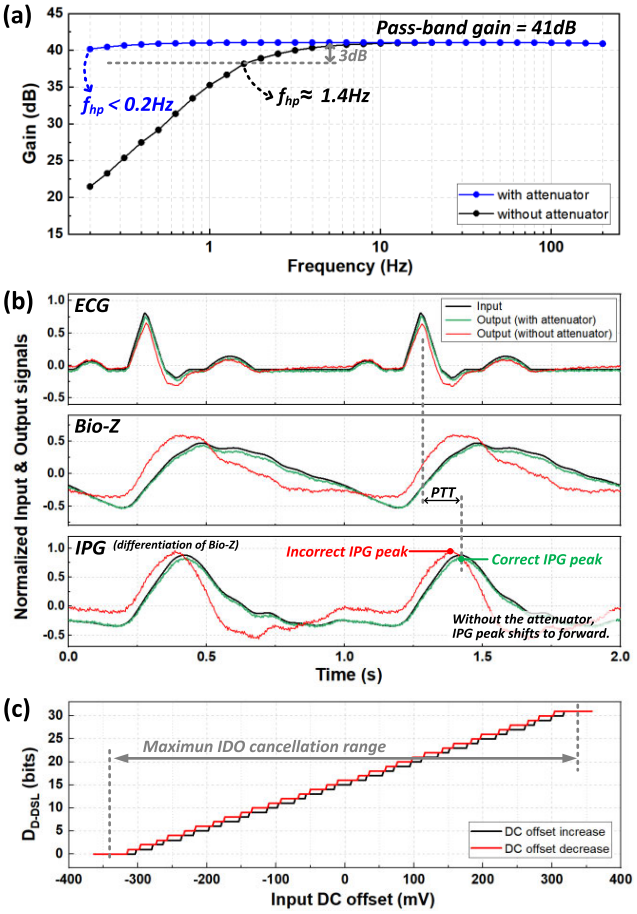

FIGURE 9. (a) Frequency response of the low-noise amplifier in biopotential AFE with a proposed attenuator. (b) Measured ECG and IPG waveforms on an activation and deactivation conditions of the attenuator. (c) Maximum input DC offset cancellation range of the hybrid-DSL in biopotential AFE.

0.2Hz by activating the attenuator. Fig.9(b) shows bio-signal waveforms on a deactivation and activation conditions of the attenuator, where the IPG waveform was obtained by differentiating the bio-impedance waveform. Since ECG peak has a high frequency, the measured ECG peaks are located on a same position in both conditions. However, phase shift occurs on the bio-impedance waveform in the deactivated attenuator condition which causes the incorrect IPG peak position, and it was eliminated by activating the attenuator which enables to find an accurate PTT. Fig.9(c) shows a DC-cancellation range of the LNA using the hybrid-DSL, where the digital-DSL compensates for the most IDO by adjusting the D_{D-DSL} and analog-DSL only compensates the remained small IDO. The maximum DC-cancellation range is about -340mV to $+340$mV, and as shown in the black and red results, the hybrid-DSL operates in hysteresis due to co-working of the analog/digital-DSLs.

Fig.10 shows an input-referred noise performance of the biopotential AFE, where the integrated noise was achieved to $0.69\mu V_{rms}$ from the frequency range of 0.5Hz to 100Hz.

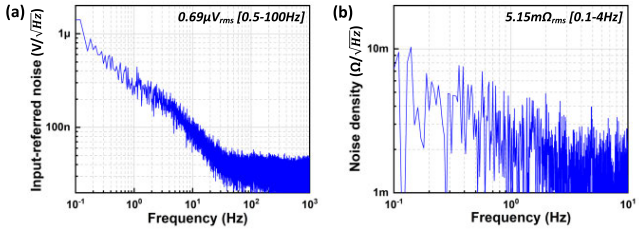

FIGURE 10. Noise performances of (a) the biopotential and (b) bio-impedance AFEs.

Fig.10(b) shows the input-referred noise density of the bio-impedance AFE, which achieved the integrated impedance noise of 5.15mΩ_{rms} from 0.1Hz to 4Hz. Each AFEs precisely measured the ECG and IPG signals based on these noise performances.

B. CONTINUOUS BP MONITORING AND PTT-BP ESTIMATION

Fig.11(a) is a photograph of wearing the neck-band device, and fig.11(b) is continuous monitoring window in the PC Matlab. Measured ECG and IPG waveforms and calculated pulse transit time are shown in the window, and estimated BP is obtained using the PTT and equation (1). Fig.11(c) shows power breakdown of the sensor module and the customized ROIC respectively, where the power consumption for the signal acquisition was minimized by implementing the ROIC. Total power consumption is 67.14mW, which enables to operate longer than 5 hours when using a 350mAh Li-poly battery. Although the Bluetooth module consumes most of the power, it can be further improved by selecting the latest ultra low-power module.

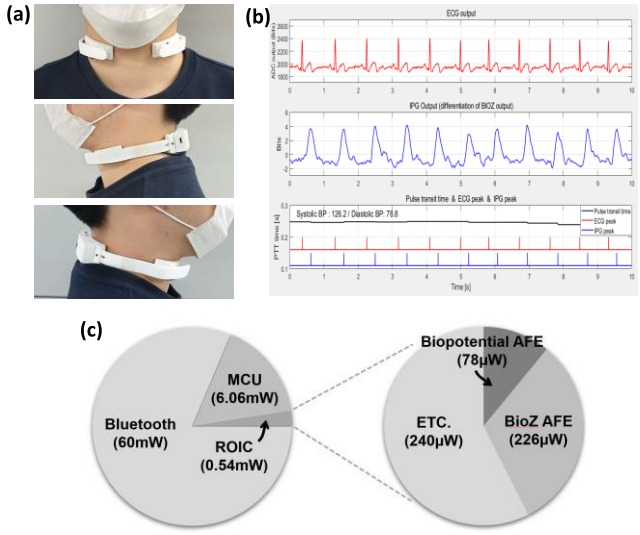

FIGURE 11. (a) Photograph for wearing the neck-band device and (b) measured bio-signals and calculated pulse transit time in a PC matlab. (c) Power breakdown of the developed sensor module and the ROIC.

Accuracy of the BP estimation was compared to measure the developed neck-band device and monitoring system. The experiment was conducted on 8 subjects of healthy men with

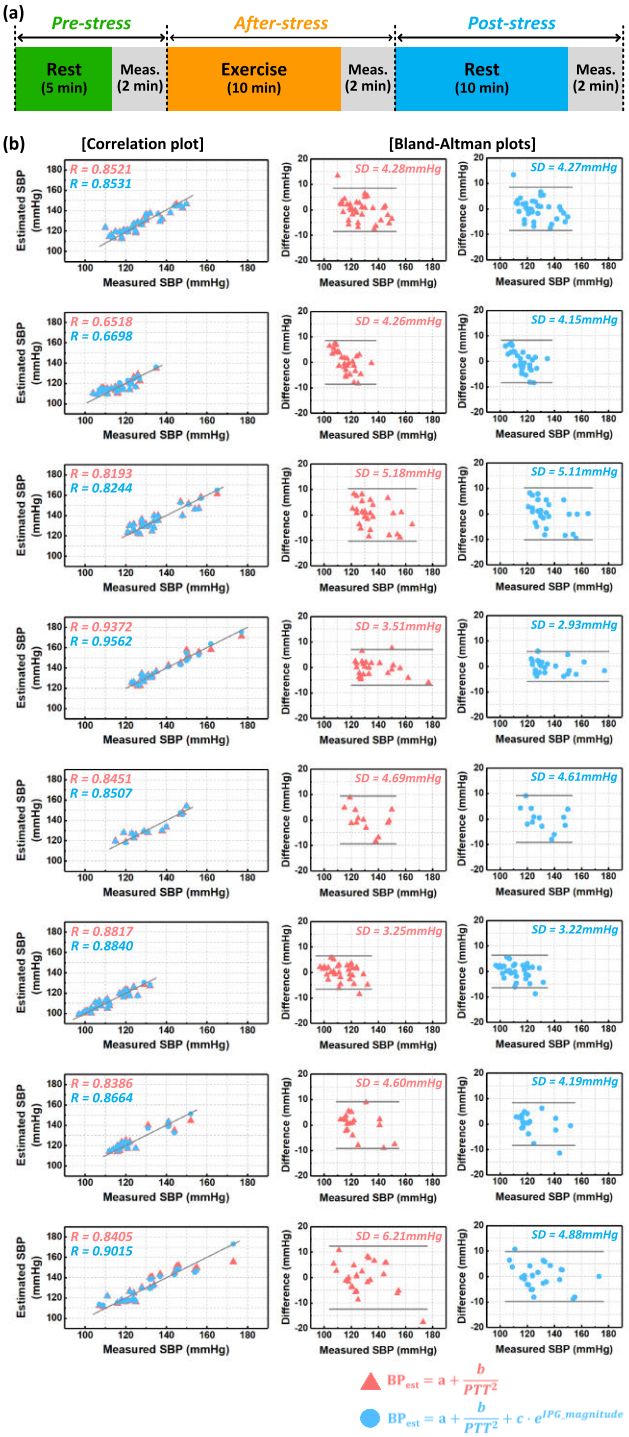

FIGURE 12. (a) Procedure to obtain simultaneously measured PTT and BP in a various physical stress condition. (b) Correlation and Bland-Altman plots between the estimated BP and reference BP for 8 subjects.

26-34 ages, and the data for each subject were obtained by repeating the measurement procedure in fig.12(a). Physical stress such as exercise significantly changes the blood pressure in a short period of time, and fig.12(a) shows a procedure for simultaneously measuring the PTT and BP und er physical stress conditions. It consists of 7 minutes

of rest, 12 minutes of exercise, and 10 minutes of restore conditions, and each step has time to measure the PTT using the neck-band device and reference BP using a commercial instrument (HEM-7121, Omron) for 2 minutes. Fig.12(b) shows the BP estimation results for 8 subjects, which are presented as a correlation on and Bland-Altman plots. While the results have correlation of 0.6518 to 0.9372 and standard deviation of 3.25 mmHg to 6.21 mmHg when the BP estimation algorithm without IPG magnitude term is used, they have correlation of 0.6698 to 0.9562 and standard deviation of 2.93 mmHg to 5.11 mmHg by using the equation (1). Mean correlation and standard deviation for 8 subjects were achieved as 0.8508 mmHg and 4.17 mmHg. The reason is that the differences in Bland-Altman plots of each subject were slightly decrease by applying the IPG magnitude term, and it is estimated that the IPG magnitude measured in the high BP range tends to be quite large due to the increased intensity of heartbeat. This experiment was conducted after obtaining informed consent for the subjects and approval from the institutional review board (IRB).

V. CONCLUSION

This work developed a neckband device to provide PTT-based continuous blood pressure monitoring using ECG and IPG signals. The attenuator-assisted hybrid-DSL scheme was proposed in the AFE design of biopotential and bio-impedance. It enabled accurate PTT acquisition by lowering the HPF cutoff frequency less than 0.2 Hz, and also compensated large input DC-artifacts up to 340 mV. This allows to acquire very small bio-signals like IPG around the neck while implementing the lead-off detection.

The efficacy of the continuous BP estimation using the developed wearable device prototype was evaluated for 8 healthy subjects under the physical stress condition, where the mean correlation coefficient and the standard deviation were achieved as 0.8508 and 4.17mmHg respectively. It reflects the wearable neckband device based on ECG and IPG around the neck could be utilized as one of the convenient and accurate continuous-BP monitoring systems. On the other hands, further works are needed to support monitoring system in portable devices such as smartphone and to verify the BP estimation for various experimental groups.

ACKNOWLEDGMENT

(Kwangmuk Lee and Yumin Kang contributed equally to this work.)

REFERENCES

[1] *IEEE Standard for Wearable Cuffless Blood Pressure Measuring Devices*, Standard 1708-2014, 2014.
[2] E. C. Chua, S. J. Redmond, G. McDarby, and C. Heneghan, "Towards using photo-plethysmogram amplitude to measure blood pressure during sleep," *Ann. Biomed. Eng.*, vol. 38, pp. 945–954, Mar. 2010.
[3] R. Gircys, A. Liutkevicius, A. Vrubliauskas, and E. Kazanavicius, "Blood pressure estimation accoording to photoplethysmographic signal steepness," *Inf. Technol. Control*, vol. 44, no. 4, pp. 443–450, Dec. 2015.
[4] K. Yuki and H. Tsuyoshi, "Sensor technology to realize continuous blood pressure monitoring," (in Japanese), *Omron Technics*, vol. 50, no. 4, pp. 26–34, 2019.
[5] L. Peter, N. Noury, and M. Cerny, "A review of methods for non-invasive and continuous blood pressure monitoring: Pulse transit time method is promising?" *IRBM*, vol. 35, no. 5, pp. 271–282, Oct. 2014.
[6] M. Sharma, K. Barbosa, V. Ho, D. Griggs, and T. Ghirmai, "Cuff-less and continuous blood pressure monitoring: A methodological review," *Technologies*, vol. 5, p. 21, Jun. 2017.
[7] E. Finnegan, S. Davidson, M. Harford, and J. Jorge, "Pulse arrival time as a surrogate of blood pressure," *Sci. Rep.*, vol. 11, Oct. 2021, Art. no. 22767.
[8] R. Lazazzera, Y. Belhaj, and G. Carrault, "A new wearable device for blood pressure estimation using photoplethysmogram," *Sensors*, vol. 19, p. 2557, Jan. 2019.
[9] A. M. Carek, J. Conant, A. Joshi, H. Kang, and O. T. Inan, "SeismoWatch: Wearable cuffless blood pressure monitoring using pulse transit time," *ACM Interact., Mobile, Wearable Ubiquitous Technol.*, vol. 1, no. 3, pp. 1–16, Sep. 2017.
[10] T. W. Wang, H. W. Chu, W. X. Chen, Y. T. Shin, P. C. Hsu, H. M. Cheng, and S. F. Lin, "Single-channel impedance plethysmography neck patch device for unobtrusive wearable cardiovascular monitoring," *IEEE Access*, vol. 8, pp. 184909–184919, 2020.
[11] T. H. Huynh, R. Jafari, and W. Y. Chung, "Noninvasive cuffless blood pressure estimation using pulse transit time and impedance plethysmography," *IEEE Trans. Biomed. Eng.*, vol. 66, no. 4, pp. 967–976, Apr. 2019.
[12] M. Konijnenburg, "A multi(bio)sensor acquisition system with integrated processor, power management, 8×8 LED drivers, and simultaneously synchronized ECG, BIO-Z, GSR, and Two PPG readouts," *IEEE J. Solid-State Circuits*, vol. 51, no. 11, pp. 2584–2595, Nov. 2016.
[13] J. Xu, M. Konijnenburg, S. Song, H. Ha, R. van Wegberg, M. Mazzillo, G. Fallica, C. Van Hoof, W. De Raedt, and N. Van Helleputte, "A 665 μW silicon photomultiplier-based NIRS/EEG/EIT monitoring ASIC for wearable functional brain imaging," *IEEE Trans. Biomed. Circuits Syst.*, vol. 12, no. 6, pp. 1267–1277, Dec. 2018.
[14] Q. Fan, F. Sebastiano, J. H. Huijsing, and K. A. A. Makinwa, "A 1.8 μW 60 nV/$\sqrt{HZ}$ capacitively-coupled chopper instrumentation amplifier in 65 nm CMOS for wireless sensor nodes," *IEEE J. Solid-State Circuits*, vol. 46, no. 7, pp. 1534–1543, Jul. 2011.
[15] H. T. Ma, "A blood pressure monitoring method for stroke management," *Biomed Res. Int.*, vol. 2014, pp. 1–7, Oct. 2014.
[16] E. M. Landis, "The capillaries of the skin: A review," *J. Invest. Dermatol.*, vol. 1, no. 4, pp. 295–311, 1938.
[17] M. Min, H. Koiv, E. Priidel, K. Pesti, and P. Annus, "Noninvasive acquisition of the aorta blood pressure waveform," in *Wearable Devices-The Big Wave of Innovation*. London, U.K.: IntechOpen, 2019.
[18] A. A. Brandao, "I Luso-Brazilian positioning on central arterial pressure," *ARQ Bras Cardiol.*, vol. 108, no. 2, pp. 100–108, Feb. 2017.
[19] T. Wang, H. Chu, L. Chou, Y. Sung, and Y. Shih, "Bio-impedance measurement optimization for high-resolution carotid pulse sensing," *Sensors*, vol. 21, no. 5, p. 1600, Feb. 2021.
[20] K. Lee, H. Y. Chae, K. Park, Y. Lee, S. Cho, H. Ko, and J. J. Kim, "A multifunctional physiological hybrid-sensing E-skin integrated interface for wearable IoT applications," *IEEE Trans. Biomed. Circuits Syst.*, vol. 13, no. 6, pp. 1535–1544, Dec. 2019.
[21] B. Oh and J. J. Kim, "A four-step incremental ADC based on double extended binary counting with capacitive DAC," *IEEE Trans. Circuits Syst. II, Exp. Briefs*, vol. 67, no. 10, pp. 1685–1689, Oct. 2020.
[22] R. F. Yazicioglu, C. V. Hoof, and R. Puers, *Biopotential Readout Circuits for Portable Acquisition System*. New York, NY, USA: Springer, 2009, p. 10.
[23] J. Nyboer, M. M. Kreider, and L. Hannapel, "Electrical impedance plethysmography: A physical and physiologic approach to peripheral vascular study," *Circulat.*, vol. 2, pp. 811–821, Oct. 1950.
[24] R. R. Harrison and C. Charles, "A low-power low-noise CMOS amplifier for neural recording applications," *IEEE J. Solid-State Circuits*, vol. 38, no. 6, pp. 958–965, Jun. 2003.
[25] H. Chandrakumar and D. Marković, "A high dynamic-range neural recording chopper amplifier for simultaneous neural recording and stimulation," *IEEE J. Solid-State Circuits*, vol. 52, no. 3, pp. 645–656, Mar. 2017.
[26] *Understanding Lead-Off detection in ECG*, Texas Instruments, Dallas, TX, USA, May 2012.
[27] J. Xu, S. Mitra, C. Van Hoof, R. F. Yazicioglu, and K. A. A. Makinwa, "Active electrodes for wearable EEG acquisition: Review and electronics design methodology," *IEEE Rev. Biomed. Eng.*, vol. 10, pp. 187–198, 2017.

KWANGMUK LEE (Student Member, IEEE) received the B.S. degree in electrical and computer engineering from the Ulsan National Institute of Science and Technology (UNIST), Ulsan, South Korea, in 2015, and the joint master's and Ph.D. degree from the Department of Electrical Engineering, UNIST, in 2021. Since 2021, he has been with Samsung Electronics Device Solutions. His research interests include healthcare system design, in particular CMOS biomedical circuits.

YUMIN KANG received the joint B.S. and M.S. degree from the Department of Mechanical and Biomedical Engineering and the Division of Mechanical Mechatronics Engineering, Kangwon National University, Chuncheon, South Korea, in 2015, and the Ph.D. degree in biomedical science and engineering from Hanyang University, Seoul, South Korea, in 2022. His research interests include healthcare system design, in particular bio-signal analysis.

CHAN SAM PARK (Student Member, IEEE) received the B.S. degree in electrical and computer engineering from the Ulsan National Institute of Science and Technology, Ulsan, South Korea, in 2017, where he is currently pursuing the joint master's and Ph.D. degree with the Department of Electrical Engineering. His research interests include healthcare system design, in particular CMOS biomedical ROIC and data converters.

HYUNJOONG KIM (Student Member, IEEE) received the B.S. degree in electrical engineering from the Ulsan National Institute of Science and Technology (UNIST), Ulsan, South Korea, in 2019, where he is currently pursuing the Ph.D. degree in electrical engineering. His research interests include healthcare system design, in particular low power analog and mixed-signal circuits for biomedical ICs.

DAE SIK KEUM received the B.S. degree in computer science and the master's degree in computer engineering from Dongguk University, Seoul, South Korea, in 1993 and 1996, respectively. From 1996 to 2005, he was a System Engineer with several MRI Company (MEDISON, CHI, and MEDINUS), Daejeon or Seoul. From 2005 to 2014, he was a H/W Team Leader in industrial embedded and robot controller with DAIN CUBE, Seoul. Since 2014, he has been a Research Team Leader at SOSO Company Ltd. His research interests include H/W and systems for wearable healthcare devices, bio-signal measurement equipment, and consumer electronics.

DONG PYO JANG received the B.S. and M.S. degrees in electronic engineering and the Ph.D. degree in biomedical engineering from Hanyang University, Seoul, South Korea, in 1996, 1998, and 2002, respectively. He has extensive research expertise in the broad area of biomedical engineering and more specifically in the areas of physiological data analysis, in vivo neuroimaging, and electrochemistry. He is currently the Director of the Neural Engineering Laboratory and a Full Professor with Hanyang University.

JAE JOON KIM (Senior Member, IEEE) received the B.S. degree in electronic engineering from Hanyang University, Seoul, South Korea, in 1996, and the M.S. and Ph.D. degrees in electrical engineering from the Korea Advanced Institute of Science and Technology, Daejeon, South Korea, in 1998 and 2003, respectively. From 2000 to 2001, he was with Berkana Wireless Inc., San Jose, CA, USA (now merged into Qualcomm, Inc.), where he was involved in designing wireless transceivers. From 2003 to 2005, he was with Hynix Semiconductor, Seoul, where he was involved in wireless transceivers and smart-card controllers. From 2005 to 2011, he was the Deputy Director with the Ministry of Information and Communications, Korean Government, and the Ministry of Trade, Industry and Energy. From 2009 to 2011, he was a Research Engineer II with the Georgia Institute of Technology, Atlanta, GA, USA. Since 2011, he has been an Associate Professor with the Ulsan National Institute of Science and Technology, Ulsan, South Korea. His research interests include integrated circuits and systems for smart sensor interfaces, wearable healthcare devices, consumer electronics, automotive electronics, and wireless transceivers.